JOURNAL OF MECHANICAL ENGINEERING, SCIENCE, AND INNOVATION
ITATS
Research Article

CFD-Validated Kriging Surrogate for Multi Objective Aerodynamic Optimization of a Go-Kart Drag-Lift Pareto Front under Pitching Moment Constraint

Journal of Mechanical Engineering, Science, and Innovation
e-ISSN: 2776-3536
2026, Vol. 6, No. 1
DOI: 10.31284/j.jmesi.2026.v6i1.8742
ejurnal.itats.ac.id/jmesi

Ahmad Al Kafi[1] and Ahmad Atif Fikri[1*]

[1]Department of Mechanical and Industrial Engineering, State University of Malang, Indonesia

Corresponding author:
Ahmad Atif Fikri
Department of Mechanical and Industrial Engineering, State University of Malang, Malang, 65146, Indonesia
Email: atif.fikri.ft@um.ac.id

Abstract

Go-kart aerodynamics involves a trade-off between drag reduction, lift control, and longitudinal stability, yet most previous studies do not explicitly constrain pitching moment during design optimization. This study proposes a CFD-validated Gaussian Process Regression (Kriging) surrogate for multi objective aerodynamic optimization of go-kart bodywork using ground clearance, nose angle, and operating speed as design variables. A 25-point maximin Latin hypercube design was evaluated using steady RANS CFD, and the surrogate was used to construct a drag-lift Pareto front under an uncertainty-aware pitching moment constraint at 65 km/h. The recommended knee point design (h = 40 mm, α = 24.79°) achieved Cd = 0.771, Cl = 0.157, and Cm.pitch = 0.171. Compared with the baseline, it reduced lift and pitching moment by about 35% each, with a 4.6% drag penalty. Additional CFD checks at 42 and 89 km/h confirmed that the selected design remained feasible and stable across the operating range. These results demonstrate that surrogate-assisted, stability-constrained optimization can identify practically viable go-kart configurations that improve aerodynamic stability without a large drag penalty, providing a useful framework for bodywork tuning within the studied design range.

Keywords: *Aerodynamic optimization, CFD validation, Gaussian process regression, Go-kart, Pareto front.*

Received: February 15, 2026; Received in revised: April 15, 2026; Accepted: April 16, 2026
Handling Editor: Naili Saidatin and Nima Vaziri

INTRODUCTION

Go-karts are widely used for racing and recreational driving, where aerodynamic efficiency becomes increasingly important as speed rises [1]. Typical operating speeds

range from approximately 45 to 90 km/h. At the upper end of this range, aerodynamic instabilities pose a genuine safety risk, and rear devices such as spoilers are reported to be necessary to prevent a go-kart from becoming airborne at speeds of 80 km/h or higher[2]. While the compact geometry and modest speeds sometimes lead aerodynamics to be deprioritized, Computational Fluid Dynamics (CFD)-based studies confirm that small bodywork-driven drag reductions can translate into measurable lap-time gains[3], making systematic evaluation of drag-lift trade-offs and stability related pitching moments under realistic ride-height constraints practically relevant[1-4].

CFD is a suitable tool for evaluating drag, lift/downforce, and stability-related moment effects, but high-fidelity simulation becomes computationally expensive when applied iteratively across a design space. To ensure credibility of steady Reynolds-Averaged Navier-Stokes (RANS) predictions for bluff-body wakes, validation against benchmark geometries is common[5-6]. Ahmed body is widely used as a reference case for RANS modeling and has extensive published aerodynamic data, making it suitable for validating solver settings and meshing strategy before applying CFD to vehicle like bodies[7-8]. To reduce computational cost while still exploring trade-offs, surrogate-based optimization is frequently adopted, combining space-filling sampling with Kriging/Gaussian-process regression to approximate CFD responses efficiently[9-11]. In particular, Latin Hypercube Sampling (LHS) is a standard space-filling DOE approach[12], and maximin-type criteria are widely used to enhance coverage by spreading design points more uniformly in the input space[13-14].

Existing go-kart CFD studies have primarily focused on drag reduction or general aerodynamic characterization[1, 2, 3], without coupling multi-objective optimization to an explicit pitching moment constraint that enforces longitudinal stability throughout the design search. Furthermore, prior surrogate-based vehicle aerodynamic optimization studies have rarely integrated a robust, uncertainty-aware constraint formulation that accounts for Gaussian Process Regression (GPR) prediction uncertainty when screening feasible designs. The present work addresses both gaps simultaneously. This study presents a CFD-validated Kriging surrogate framework for multi objective aerodynamic optimization of a go-kart bodywork parameterization, targeting the drag-lift trade-off while explicitly enforcing longitudinal stability through a pitching moment constraint. A 25-point maximin LHS design over ground clearance, nose angle, and operating speed was simulated using steady RANS CFD to train surrogate models for the drag coefficient (Cd), lift coefficient (Cl), and pitching moment coefficient (Cm.pitch). The surrogates enable dense exploration and construction of a constrained Cd-Cl Pareto front under a robust pitching moment constraint. Verification was performed by re-simulating representative Pareto candidates in CFD and evaluating robustness across additional operating speeds within the relevant range.

Aerodynamic Coefficient and Optimization Formulation

Aerodynamic performance is quantified using non-dimensional coefficients derived from aerodynamic forces and moments, enabling consistent comparison across geometries and operating speeds. Following standard vehicle aerodynamics practice and definitions adopted in go-kart CFD studies, drag and lift force are expressed as Eq. (1) and Eq. (2):

$$F_{drag} = \frac{1}{2}\rho C_d V^2 A \quad (1)$$

$$F_{lift} = \frac{1}{2}\rho C_l V^2 A \quad (2)$$

where ρ is air density (kg/m^3), V is the vehicle speed (m/s), and A is the reference frontal area (m^2)[1].

The aerodynamic coefficients are computed as $C_d = 2F_{drag}/\rho V^2 A$ and $C_l = 2F_{lift}/\rho V^2 A$. In this study $C_l > 0$ denotes upward lift and $C_l < 0$ denotes downforce[1]. Longitudinal stability is represented by the pitching moment coefficient:

$$Cm_{pitch} = \frac{M_{pitch}}{\frac{1}{2}\rho V^2 A L_{ref}} \quad (3)$$

where M_{pitch} is the pitching moment about the selected reference point (N·m) and L_{ref} is a characteristic reference length (m).

Based on the aerodynamic coefficients defined above, the design problem is formulated as a multi-objective optimization problem. The objective is to simultaneously minimize drag and lift while satisfying a pitching moment constraint that enforces longitudinal stability throughout the design space. Let the design vector be $\mathbf{x} = [h, \alpha, V]$, where h is the ground clearance (mm), α is the nose pitch angle (degrees), and V is the operating speed (km/h), which is included as an input for consistent surrogate training across the operating envelope. The multi-objective problem is then formulated as Eq. (4) dan Eq. (5):

$$\min_x f1(x) = C_d(x) \quad (4)$$

$$\min_x f2(x) = C_l(x) \quad (5)$$

subject to a pitching moment feasibility requirement. Because GPR provides not only a predicted mean but also a prediction uncertainty standard deviation at each **x**, it supports uncertainty-aware decision-making in constrained design[9-10].

The robust pitching moment constraint is written as Eq. (6):

$$g(x) = \mu C_m(x) + \kappa\sigma C_m(x) - C_{m,bound} \leq 0 \quad (6)$$

where $\mu_{C_m}(\mathbf{x})$ and $\sigma_{C_m}(\mathbf{x})$ are the surrogate-predicted mean and standard deviation of $C_{m.\text{pitch}}$, $C_{m.\text{bound}}$ is the allowable pitching moment limit, and k controls constraint conservativeness [15-16]. Larger k values yield safer solutions by requiring a wider margin to the constraint boundary, while smaller k values increase design freedom but may raise the probability of constraint violation when the surrogate is imperfect[9, 15].

METHODS AND ANALYSIS

Overall research workflow adopted in this study is shown in figure 1, covering CFD-based data generation, surrogate model training, constrained multi-objective optimization, and CFD verification.

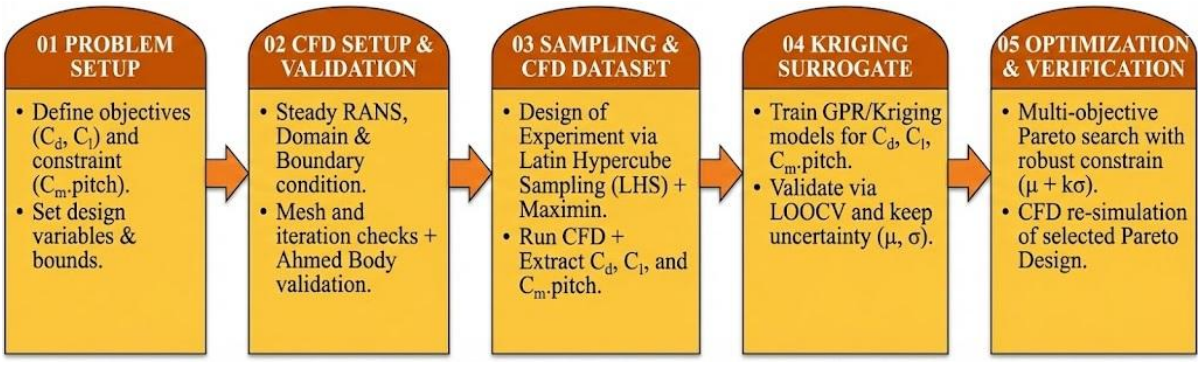

Figure 1. Research workflow

Table 1. Design variables and bounds used for DOE, surrogate training, and optimization

No.	Variable	Symbol	Unit	Bounds
1	Freestream speed	V	km/h	42 ≤ V ≤ 89
2	Ground clearance	h	mm	25 ≤ h ≤ 40
3	Nose pitch angle	α	Deg (°)	20 ≤ α ≤ 30

Table 2. Go-kart geometry specifications and reference quantities

No.	Parameter	Value	Note
1	Overall dimensions (L x W x H)	1.70 x 1.10 x 0.515 m	-
2	Wheelbase	1.06 m	-
3	Frontal reference area (A)	0.346 m^2	Projected frontal area from CAD
4	Reference length (L_{Ref})	1.70 m	Characteristic length for Cm.pitch normalization
5	Air density (ρ)	1.225 kg/m^3	Standard sea-level value

Design Variables, Bounds, and Reference Quantities

The CFD dataset was constructed by varying speed (V), ground clearance (h), and nose angle (α) within bounds selected to reflect a realistic operational envelope and FIA legal bodywork adjustments. Table 1 lists the design variables and their bounds, which are consistent throughout the DOE, surrogate training, and Pareto construction phases.

Go-kart geometry was constructed from the CAD model. Key geometric and reference quantities used for coefficient post-processing are listed in Table 2. The frontal reference area A and pitching moment reference length L_{Ref}were extracted directly from the CAD model using consistency checks with the stored dimensional force and moment data in the CFD database.

Maximin Latin Hypercube Sampling

To efficiently explore the three-dimensional design space under a limited CFD budget, a 25-point maximin LHS scheme was employed. The LHS-maximin strategy ensures uniform one-dimensional projections while maximizing the minimum pairwise inter-point distance, improving surrogate conditioning for nonlinear responses[12-14]. Each input variable was normalized to the unit hypercube as Eq. (7):

$$\tilde{x}_i = \frac{x_i - x_{i,min}}{x_{i,max} - x_{i,min}}, i \in \{V, h, \alpha\} \quad (7)$$

The training set of N = 25 CFD-evaluated points is used to train all three surrogate models.

CFD Model Setup

All aerodynamic evaluations were performed using STAR-CCM+ 23.06 with a steady, incompressible Reynolds-Averaged Navier-Stokes (RANS) approach in an external flow computational domain which is shown in Figure 2. The go-kart CAD geometry was positioned inside a sufficiently large computational domain to minimize blockage and to allow the wake to develop downstream. The upstream boundary was prescribed as a velocity inlet using the target freestream speed V, and the downstream boundary set as a pressure outlet at zero gauge pressure. The top and lateral boundaries were treated as slip walls and were placed sufficiently far from the body to minimize blockage. No symmetry plane was applied. The full domain was simulated. Go-kart bodywork surface was treated as a no-slip wall.

The turbulence closure and near-wall treatment were fixed after validation on the Ahmed-body benchmark and subsequently held constant for all go-kart DOE and verification runs to ensure database consistency. The k-ω SST turbulence model was adopted as the standard choice for external aerodynamics with separated flows, combined with second-order spatial discretization to improve accuracy of force and moment predictions[17].

Table 3. Steady RANS CFD setup

No.	Item	Setting	Note
1	CFD solver	STAR-CCM+ 23.06	Version stated for reproducibility
2	Solver type	Pressure-based, steady	Incompressible external aerodynamics at kart speeds
3	Turbulence model	k-ω SST	Fixed after Ahmed-body validation
4	Pressure-velocity coupling	SIMPLE	Stable convergence for steady RANS
5	Spatial discretization	Second-order (pressure & momentum)	Reduces numerical diffusion in wake prediction
6	Iterations per case	500	Consistent stopping criterion across DOE and verification runs
7	Upstream boundary	Velocity inlet	Freestream speed specified at inlet
8	Downstream boundary	Pressure outlet	Zero gauge pressure at outlet
9	Top/side boundaries	Slip walls	Far-field treatment; placed to minimize blockage
10	Bottom boundary	No-slip wall	Stationary ground; consistent baseline simplification
11	Symmetry treatment	Full domain	Full geometry, no symmetry plane applied
12	Go-kart body surface	No-slip wall	Standard solid-wall boundary condition

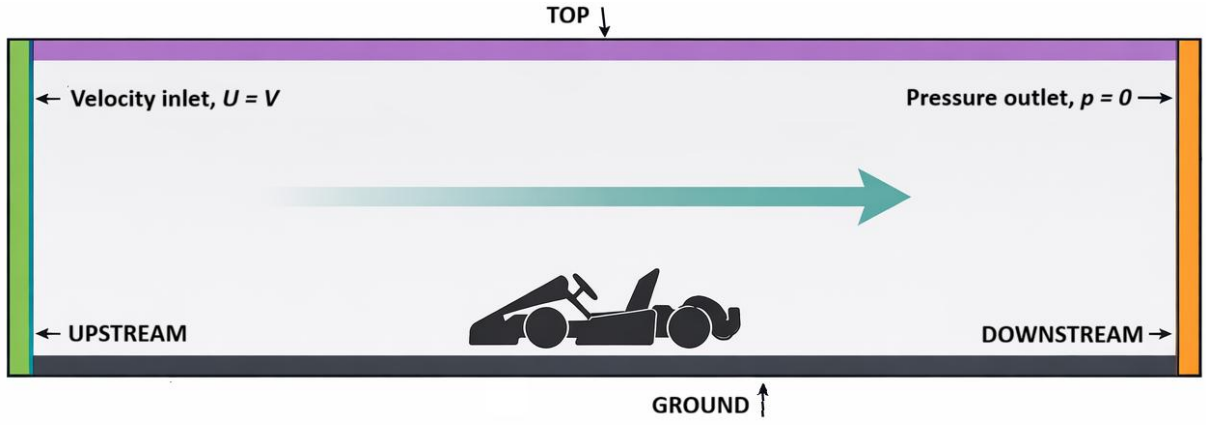

Figure 2. Schematic of the external-flow computational domain and boundary conditions for go-kart simulations

Table 4. Go-kart mesh-independence assessment case (V = 65 km/h, h = 37 mm, α = 29°)

Mesh level	Cell count	Base size	Cd	Cl	Cm.pitch	ΔCd vs finer	ΔCl vs finer	ΔCm vs finer
	(M)	(mm)				(%)		
Coarse	0.646	200	7.472201e-01	2.397249e-01	2.598603e-01	7.36	21.73	2.56
Medium	0.889	100	7.423590e-01	2.328217e-01	2.586451e-01	6.66	18.23	2.08
Fine	2.912	50	6.960142e-01	1.969307e-01	2.533811e-01	-	-	-

Meshing Strategy, Near-Wall Treatment, and Convergence Monitoring

A consistent meshing strategy was applied across all DOE cases to avoid introducing re-meshing bias into the surrogate training data. The medium mesh setting used a global base size of approximately 100 mm, with local refinements applied in go-kart bodywork. Inflation layers applied on all solid surfaces of the kart geometry, including the body, nose, and underbody panels, to resolve the turbulent boundary layer with sufficient near-wall resolution for the k-ω SST turbulence model. The prism-layer configuration comprised 15 layers with a first-layer height of 0.15 mm and a growth rate of 1.2, targeting a y^+ distribution consistent with the chosen near-wall treatment. The resulting area-weighted mean y^+ on the kart body surface was 1.8, with values remaining in the range 0.6-3.5 across the body surface. These values are compatible with the k-ω SST wall treatment applied in STAR-CCM+ 23.06, which requires $y^+ \leq 5$ for accurate near-wall resolution without wall functions.

Mesh sensitivity was assessed using three refinement levels at the baseline go-kart configuration. The Cl deviation of 18.23% between the medium and fine mesh is larger than those for Cd (6.66%) and Cm.pitch (2.08%), which is consistent with the known sensitivity of lift prediction to near-wall resolution in steady RANS frameworks[6]. Given that design selection is ultimately confirmed by direct CFD re-simulation of all Pareto candidates rather than relying solely on surrogate predictions, the medium mesh is considered adequate for constructing a consistent surrogate training database within the available computational budget. The medium mesh (0.889 million cells, 100 mm base size) was therefore applied uniformly across all DOE and verification cases.

Convergence was assessed using both residual histories and force/moment monitors. Each run was accepted into the database only after the residuals reached a stable plateau and the monitored Cd, Cl, and Cm.pitch values showed negligible drift over the final 100 iterations. All DOE and verification simulations were executed for 500 iterations under identical numerical settings, ensuring consistent sampling quality.

CFD Validation Using Ahmed-Body Benchmark

Prior to applying CFD to the go-kart configurations, the solver settings and near-wall modeling were validated against the Ahmed body benchmark, a canonical bluff-body geometry with extensive wind tunnel measurements and wide adoption for RANS validation[7]. The 25° slant-angle configuration was selected because it exhibits a separated wake and rear-surface pressure interaction representative of vehicle-like flows[7-8]. The Ahmed body was placed in an external-flow computational domain, with domain dimensions expressed as multiples of the body length L. Mesh independence was confirmed through a three-level refinement study, and y^+ distributions on the body and ground surfaces were verified to be consistent with the k-ω SST near-wall treatment requirements. The qualitative wake structure and pressure distribution patterns obtained from the CFD model were consistent with published descriptions of the 25°

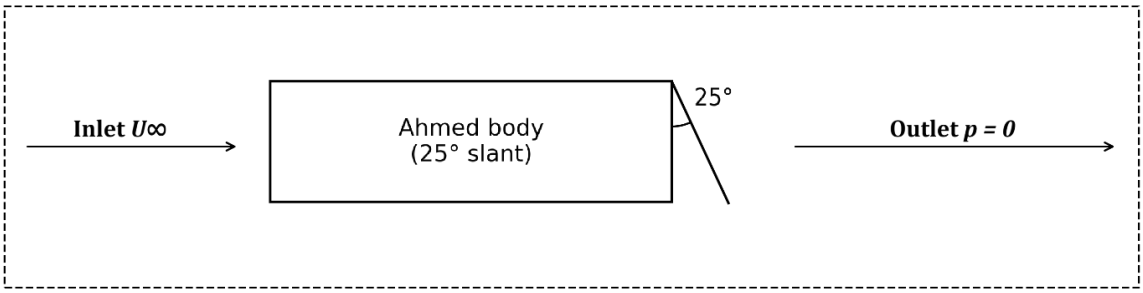

Figure 3. Ahmed-body benchmark

Ahmed-body flow behavior[7-8], and the same solver settings were subsequently applied to all go-kart simulations.

Gaussian Process Regression (GPR) Surrogate Modeling

Separate GPR surrogate models were trained for Cd, Cl, and Cm.pitch using the 25-point CFD database. The input matrix X = [V, h, α] was standardized to zero mean and unit variance prior to training to improve kernel conditioning. For each target response, the best-performing kernel was selected based on leave-one-out cross-validation (LOOCV) root-mean-square error (RMSE) from two candidates, the squared-exponential (radial basis function, RBF) kernel and the Matérn ν = 2.5 kernel[9-10]. Given a training set (X, y), the GPR predictive distribution at a new input x* is Gaussian with mean μ(x*) and variance σ^2(x*)[9-10].

$$\mu(x) = k_*^T(K + \sigma_n^2 I)^{-1}y, \sigma^2(x) = k(x,x) - k_*^T(K + \sigma_n^2 I)^{-1}k_* \quad (8)$$

where K is the kernel matrix between training points, and k_* is the vector of kernel evaluations between x and the training set. Hyperparameters $(\sigma_f, \ell_j, \sigma_n)$ were optimized by maximizing the log marginal likelihood with multiple optimizer restarts. Surrogate quality was assessed by LOOCV, reporting mean absolute error (MAE), root-mean-square error (RMSE), and coefficient of determination (R^2). Empirical ±2σ coverage was computed to verify the reliability of the predictive uncertainty band, following standard GPR evaluation practice[9-10].

Multi Objective Optimization Under a Robust Pitching Moment Constraint

Multi objective optimization was formulated to reveal the trade-off between aerodynamic efficiency and vertical force behavior, as defined in Equations (4)-(6) above. To reduce the probability of constraint violation due to surrogate approximation error, the robust constraint form (Eq. (6)) was enforced using κ = 2, corresponding to a conservative 2σ safety margin[15-16]. The Pareto set was constructed by dense surrogate sampling at fixed V = 65 km/h through: (i) feasibility filtering using Eq. (6), and (ii) non-dominated sorting in the (Cd, Cl) objective plane using standard Pareto dominance[18-19]. Candidate solutions for CFD verification were selected from the front, including the knee point and a drag-focused feasible alternative.

CFD Verification and Multi-Speed Validation Protocol

To confirm that surrogate-based recommendations transfer to high fidelity CFD, a dedicated verification set was defined. Six Pareto candidates at V = 65 km/h were resimulated by CFD, and the CFD outputs were compared against surrogate predictions for Cd, Cl, and Cm.pitch using absolute and relative errors. The percentage change relative to the baseline is computed as Eq. (9):

$$\Delta y(\%) = (y_{\text{baseline}} - y_{\text{design}})/y_{\text{baseline}} \times 100 \quad (9)$$

For robustness testing, the recommended knee design was evaluated at two additional speeds (V = 42 and 89 km/h), and the resulting coefficients were checked against the pitching moment constraint and expected speed trends. All verification simulations used the same CFD setup as the DOE database.

RESULTS AND DISCUSSIONS

CFD Response Overview and Baseline Behavior

Maximin LHS CFD database with 25 case spans V = 42-89 km/h, h = 25-40 mm, and α = 20-30°, covering typical short-circuit operating conditions and FIA-legal bodywork adjustments. The resulting aerodynamic coefficient ranges are summarized in Table 5. Positive Cl throughout the training set indicates net upward lift, which is unfavorable for vertical tire loading and stability

For improvement quantification and discussion at the design speed used for Pareto construction, case 014 at V = 65 km/h, h = 37 mm,and α = 29° is adopted as the baseline. Although this configuration achieves low drag with Cd = 0.7367, it produces relatively high lift Cl = 0.2419 and a large nose up pitching moment with Cm.pitch = 0.2618. The pitching moment exceeds the adopted stability limit Cm.bound = 0.231, confirming that drag focused tuning alone can conflict with longitudinal stability and motivating the constrained multi objective treatment.

Surrogate Model Quality and Uncertainty Assessment

LOOCV metrics for all three GPR surrogates are listed in Table 6 and visualized in Figure 4. Cd and Cm.pitch are captured with high fidelity, while Cl achieves moderate accuracy (R^2 = 0.826). This is considered acceptable for trade-off exploration, the absolute RMSE of 0.0114 is small relative to the Cl training range (approximately 10%), the Pareto front ordering is preserved across all six CFD-verified candidates, and final design selection is always confirmed by direct CFD re-simulation. The wider Cl scatter arises because lift is more sensitive to subtle pressure-field and underbody flow variations than drag, within the fixed steady RANS framework[6].

Residual diagnostics in Figure 4 show that prediction errors are centered near zero without strong systematic for any of the three responses. As expected for a space-filling DOE, GPR prediction uncertainty is lowest near the interior of the design space and increases toward the boundaries[9-10], motivating the robust constraint formulation in Eq. (6).

Constrained Pareto Front at V = 65 km/h

After dense surrogate sampling at V = 65 km/h, candidate points were filtered by the robust pitching moment requirement (μCm + 2σCm ≤ 0.231) and then non dominated sorted in the Cd and Cl objective plane. Figure 5 shows the resulting feasible region and the surrogate Pareto front with six CFD verification points. A clear trade-off is observed, reducing lift generally requires accepting higher drag.

The constrained Pareto set consistently selects the upper ground clearance limit (h = 40 mm), indicating that increased clearance manages lift and pitching moment without a disproportionate drag penalty. Along this boundary, nose angle α is the primary trade-off lever: increasing α reduces Cd but raises Cl and Cm.pitch; decreasing α lowers both stability metrics at the cost of higher drag.

Table 5. Range of aerodynamic coefficients in 25 CFD training set and baseline case

Coefficient	Min	Max	Mean	Std	Baseline (case 014)
Cd	0.7354	0.8866	0.7864	0.0424	0.7367
Cl	0.1490	0.2629	0.1942	0.0279	0.2419
Cm.pitch	0.1151	0.2787	0.1817	0.0489	0.2618

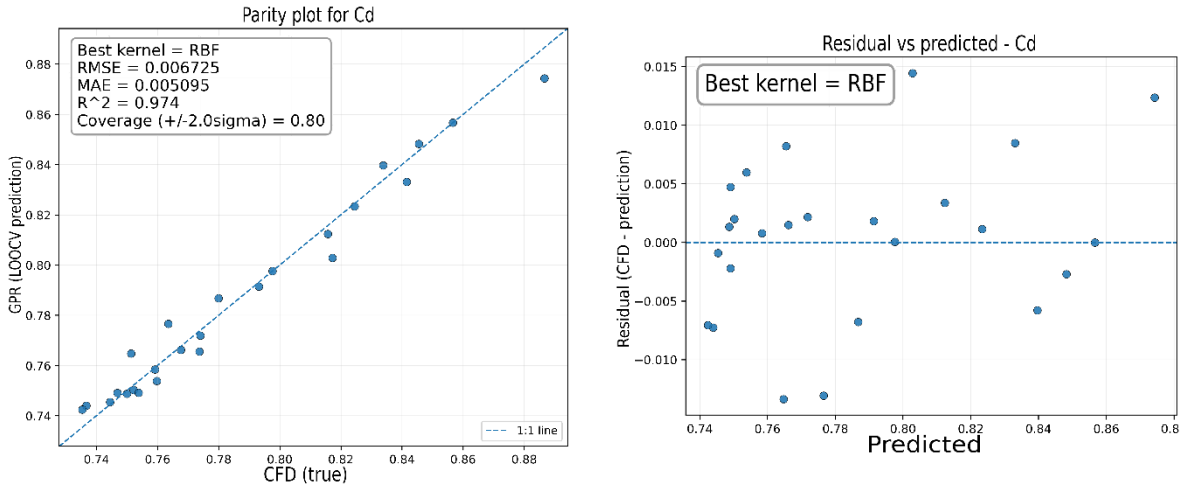

(a)

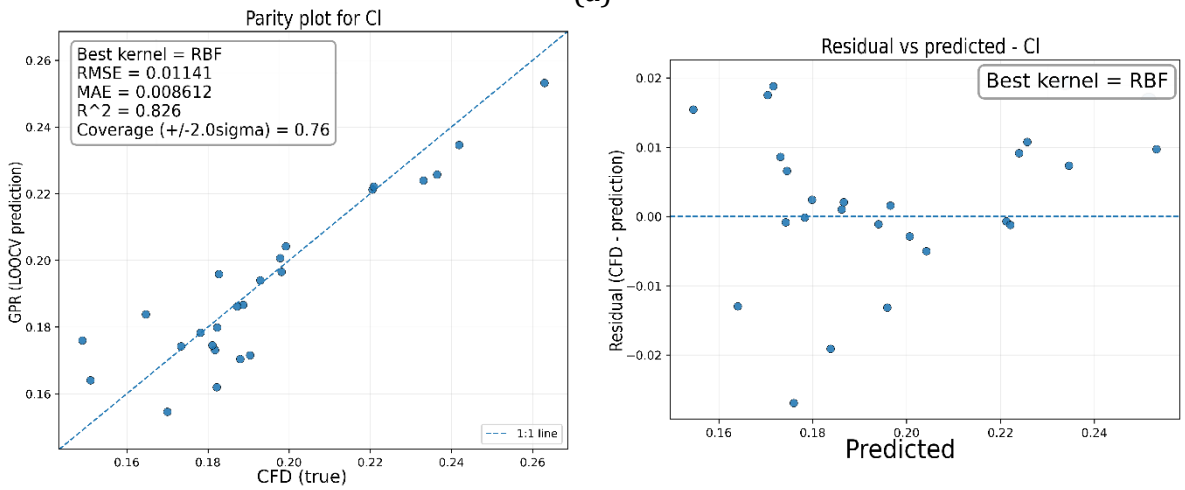

(b)

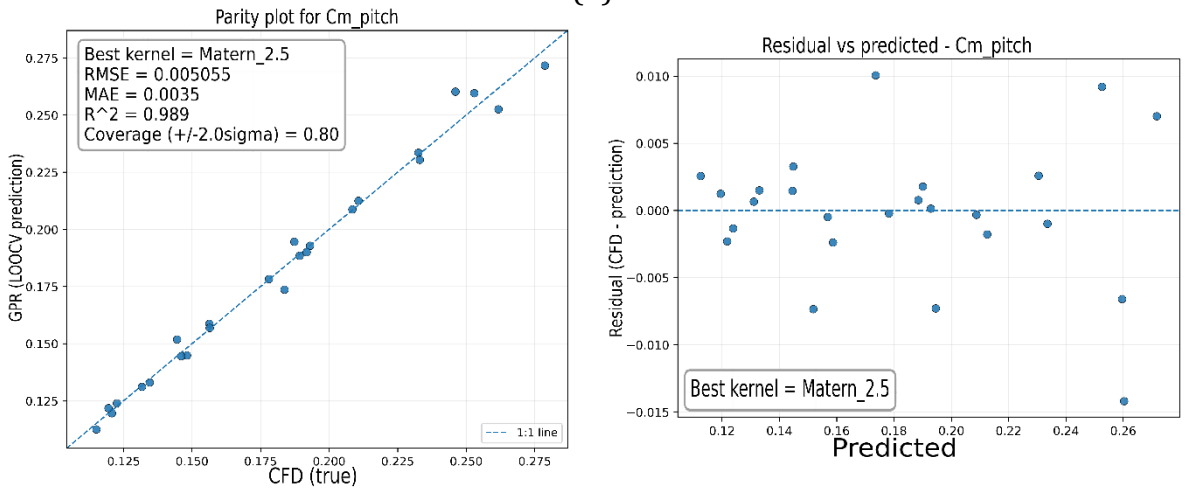

(c)

Figure 4. LOOCV parity plots and residuals vs predicted values diagnostics, (a) Cd, (b) Cl, and (c) Cm.pitch

Table 6. LOOCV metrics of the selected GPR surrogates

Target	Kernel	MAE	RMSE	R^2	Coverage (±2σ)
Cd	RBF	0.0051	0.0067	0.974	0.80
Cl	RBF	0.0086	0.0114	0.826	0.76
Cm.pitch	Matern 2.5	0.0035	0.0051	0.989	0.80

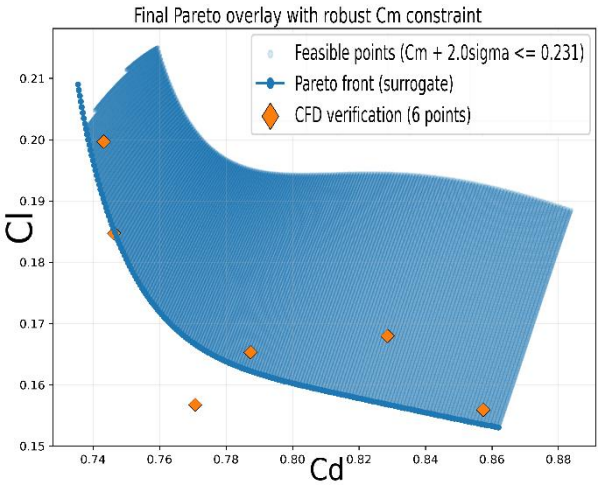

Figure 5. Final constrained Pareto overlay at V = 65 km/h

Table 7. CFD verification of six surrogate Pareto candidates

Metric	P1	P2	P3	P4	P5	P6
α (deg)	27.85	27.35	24.79	23.93	21.96	20.00
Cd (CFD)	0.7432	0.7463	0.7707	0.7874	0.8286	0.8574
Cd (GPR)	0.7354	0.7388	0.7677	0.7816	0.8192	0.8618
Cl (CFD)	0.1997	0.1847	0.1567	0.1653	0.1679	0.1559
Cl (GPR)	0.2090	0.1991	0.1678	0.1634	0.1579	0.1530
Cm (CFD)	0.2442	0.2207	0.1708	0.1611	0.1481	0.1168
Cm (GPR)	0.2329	0.2214	0.1723	0.1593	0.1337	0.1132
Cm_robust = μ+2σ	0.2393	0.2278	0.1787	0.1657	0.1398	0.1220
Robust feasible	No	Yes	Yes	Yes	Yes	Yes
CFD feasible	No	Yes	Yes	Yes	Yes	Yes

Table 8. Baseline comparison and selected designs at V = 65 km/h

Design	h	α	Cd	Cl	Cm.pitch	ΔCd vs baseline	ΔCl vs baseline	ΔCm vs baseline
	(mm)	(deg)					(%)	
Baseline	37	29.00	0.7367	0.2419	0.2618	-	-	-
Recommended	40	24.79	0.7707	0.1567	0.1708	-4.62	+35.22	+34.76
Alternative	40	27.35	0.7463	0.1847	0.2207	-1.31	+23.64	+15.70

CFD Verification of Pareto Designs and Design Selection

Table 7 compares CFD results and surrogate predictions for the six verification candidates. Cd prediction errors remain within approximately 1% across all points, confirming reliable drag-trend prediction. Lift predictions show larger deviations, but the Pareto ordering is preserved, which is sufficient for design selection followed by CFD confirmation. Point P1 slightly violates the nominal pitching moment limit in CFD, highlighting the value of the robust 2σ screening for marginal solutions.

Relative to the baseline, the recommended knee design reduces lift and pitching moment by approximately 35% each at a 4.6% drag penalty, while the alternative design offers reductions of 24% and 16%, respectively, at only a 1.3% drag cost (Table 8).

Multi-Speed Validation of the Knee Design

At both off-design speeds, Cd and Cm.pitch prediction errors remained below 1%,

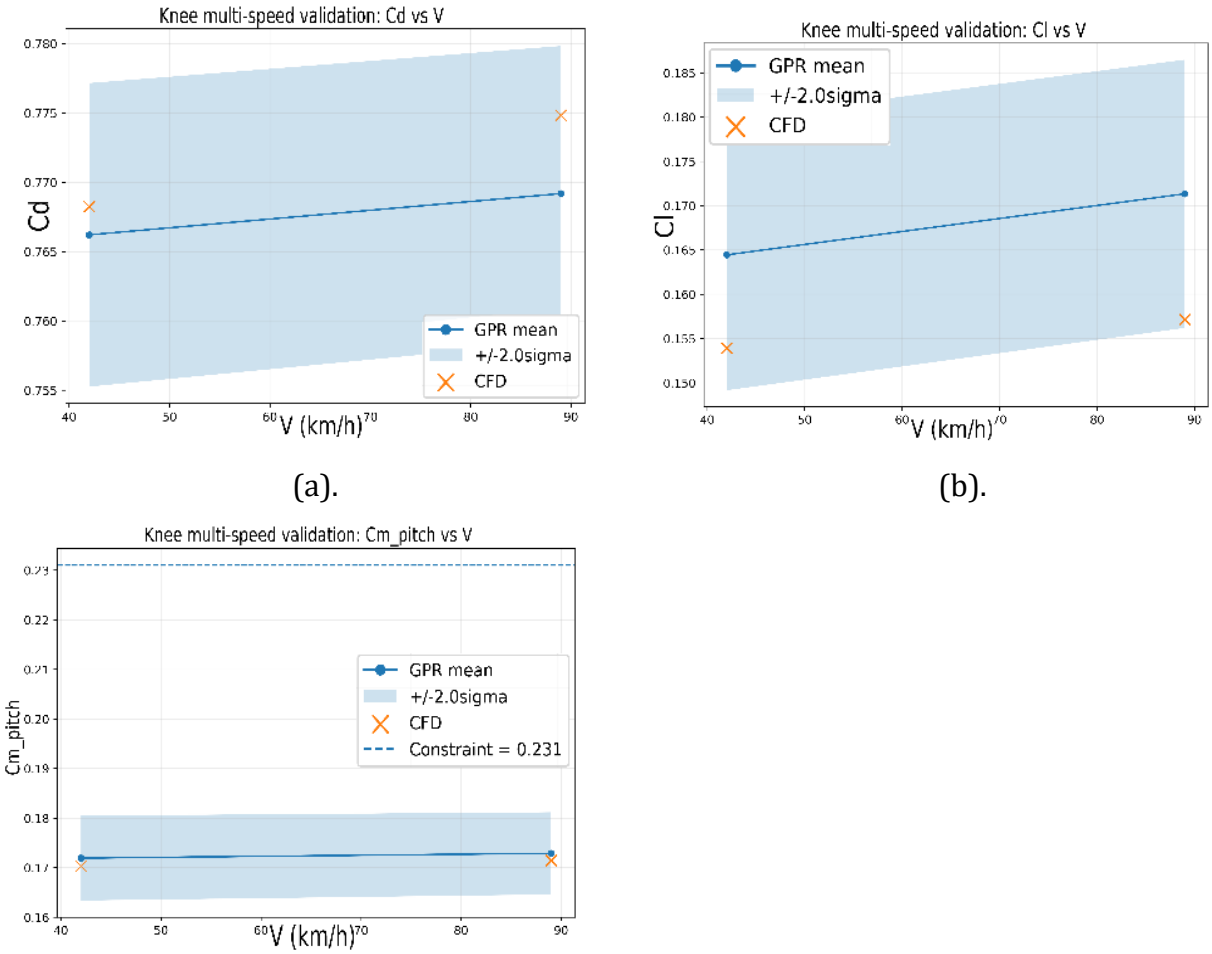

Figure 6. Multi speed validation for the knee design with comparison of GPR mean ±2σ and CFD at V = 42 and 89 km/h, (a) Cd, (b) Cl, and (c) Cm.pitch

Table 9. Comparison of CFD and surrogate predictions at V = 42 and 89 km/h

Metric	42 km/h	89 km/h
Cd (CFD)	0.7682	0.7748
Cd (GPR)	0.7662	0.7692
e_{Cd} (%)	0.27	0.73
Cl (CFD)	0.1539	0.1572
Cl (GPR)	0.1644	0.1713
e_{Cl} (%)	6.83	9.02
Cm (CFD)	0.1703	0.1715
Cm (GPR)	0.1719	0.1729
e_{Cm} (%)	0.95	0.84
Cm.robust = μ+2σ	0.1805	0.1812
Robust feasible	Yes	Yes
CFD feasible	Yes	Yes

and the robust pitching moment metric (Cm.robust ≈ 0.18) remained comfortably below the 0.231 bound, confirming sustained constraint feasibility across the operating range. Cl errors of 7-9% are consistent with the LOOCV behavior within the fixed RANS framework. These results confirm that the knee design is a broadly robust bodywork configuration throughout the explored operating envelope, not a narrow single-speed

optimum.

Aerodynamic Trends, Flow Physics and Design Implications

Across the verified Pareto points, decreasing the nose angle α drives simultaneous reductions in Cl and Cm.pitch. This behavior is consistent with reduced flow upwash and a weaker suction peak over the front bodywork. A lower nose angle deflects the oncoming flow less steeply, reducing the low-pressure region on the upper front body that generates upward lift. Simultaneously, the reduced suction near the nose lessens the nose-up pitching tendency, as the dominant pressure-lift contribution acts forward of the aerodynamic center. Conversely, the steeper front geometry at higher α values increases the effective angle of attack of the nose surface, intensifying the suction peak and the associated upward lift and pitching moment. The drag increase at lower α is consistent with stronger flow separation and a larger wake deficit as the front geometry becomes less streamlined, increasing the pressure drag component.

Figure 7 compares the surface pressure coefficient (Cp) distribution of the baseline configuration and the recommended knee design at $V = 65$km/h. The baseline shows a stronger low pressure region over the upper front body, indicating a more pronounced suction effect at the steeper nose angle. In the recommended knee design, this suction region is weakened, consistent with the reduction in lift coefficient from 0.2419 to 0.1567 and pitching moment coefficient from 0.2618 to 0.1708. In contrast, the underbody pressure distribution changes only modestly between the two cases, indicating that the reductions in Cl and Cm.pitch are mainly governed by changes in the front upper-body pressure field. The recommended design, increase the drag coefficient (Cd) by 4.6% from 0.7367 to 0.7707, consistent with a less favorable pressure recovery pattern at the lower nose angle.

The drag level of the recommended knee design (Cd = 0.771) is consistent with published go-kart CFD results, which show strong sensitivity to body geometry and driver posture [1, 3, 20]. The 4.6% drag penalty relative to the unconstrained baseline is compa-

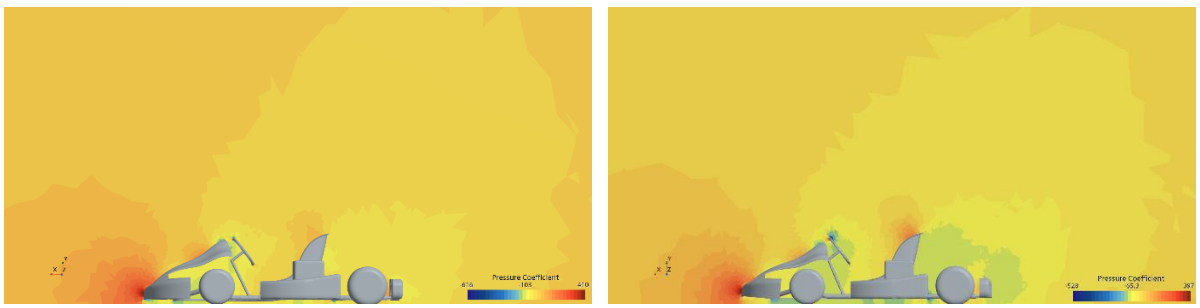

(a) (b)

Figure 7. Surface pressure coefficient (Cp) distribution at V = 65 km/h, (a) baseline design (case 014), (b) knee Design

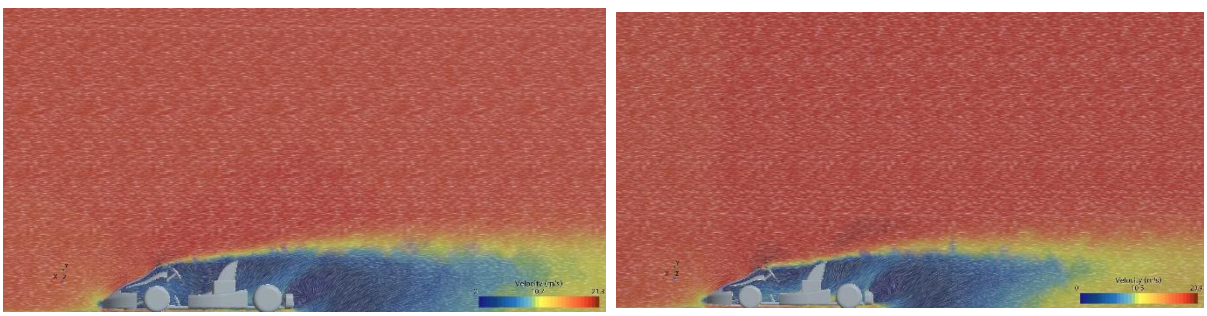

(a) (b)

Figure 8. Velocity magnitude contours, (a) baseline design (case 014), (b) knee design

able in magnitude to the 4.5% drag reduction reported by Biancolini et al. from driver-size adjustments [3], confirming that modest bodywork changes within FIA constraints can produce meaningful aerodynamic and stability effects.

For practical bodywork tuning within the studied FIA-legal range, the results indicate that maximum ground clearance combined with a moderate nose angle ($\alpha \approx 25°$) provides the most balanced aerodynamic and stability benefit. A slightly higher nose angle ($\alpha \approx 27\text{-}28°$) minimizes drag penalty but requires verification of pitching moment feasibility, whereas smaller angles ($\alpha \approx 20\text{-}23°$) further suppress lift and Cm.pitch at a substantial drag cost. All guidance applies within the studied parameterization and speed range.

This study is limited to steady-state RANS simulations at zero yaw and therefore does not capture transient aerodynamic effects relevant to cornering maneuvers or crosswind gusts. The surrogate was trained on a 25-point dataset in a three-dimensional input space, which is sufficient for smooth, low-dimensional responses but may underrepresent highly nonlinear or discontinuous behaviors.

CONCLUSIONS

This study demonstrated that a CFD-validated GPR surrogate, combined with an uncertainty-aware pitching moment constraint, enables efficient and stable multi-objective aerodynamic optimization of go-kart bodywork, a capability not achievable by conventional single-objective drag minimization. The key findings are as follows. A 25-point maximin LHS DOE over V = 42-89 km/h, h = 25-40 mm, and α = 20-30° was simulated using steady RANS CFD (STAR-CCM+ 23.06), and GPR surrogates achieved R^2 = 0.974 (Cd), 0.826 (Cl), and 0.989 (Cm.pitch). The moderate Cl accuracy is acceptable for trade-off ranking, as demonstrated by CFD re-verification of all Pareto candidates. The constrained Cd-Cl Pareto front at V = 65 km/h, built using a robust 2σ stability constraint, identified designs that the unconstrained drag-minimizing baseline (Cm.pitch = 0.262 > 0.231) could not satisfy. The selected knee-point design (h = 40 mm, α = 24.79°) achieved Cd = 0.771, Cl = 0.157, and Cm.pitch = 0.171, reducing lift and pitching moment by 35% each relative to the baseline at a 4.6% drag penalty. Multi-speed CFD checks at 42 and 89 km/h confirmed feasibility with Cd and Cm errors below 1%. Constrained solutions consistently preferred maximum ground clearance (h = 40 mm), implying that within the explored range, increased clearance mitigates pitching moment sensitivity without a disproportionate drag cost. The nose angle is the primary design lever for the drag-stability trade-off.

The framework is limited to steady RANS at zero yaw and a three-variable parameterization. Future work should incorporate yaw angle, driver posture, and additional bodywork parameters, and should validate the most promising designs experimentally or through unsteady CFD to capture transient aerodynamic effects under realistic track conditions.

ACKNOWLEDGEMENTS

The authors would like to thank the colleagues who contributed to discussions on CFD setup and surrogate modeling methodology.

DECLARATION OF CONFLICTING INTERESTS

The authors declare that there is no conflict of interest regarding the publication of this paper.

FUNDING

Thank you to PT ARJUNA ADI MAKMUR for supporting and facilitating this research.

REFERENCES

[1] F. H. Emon and A. Rahman, "Study the Aerodynamic Behaviors of a Go-Kart by using CFD Analysis," presented at the International Conference on Mechanical, Industrial and Materials Engineering 2024 (ICMIME2024), 2024.

[2] M. AL-Rawi and A. Oumssount, "One-Way Fluid Structure Interaction of a Go-Kart Spoiler Using CFD Analysis," in *The 13th Conference of the International Sports Engineering Association*, MDPI, Jun. 2020, p. 51. doi: 10.3390/proceedings2020049051.

[3] M. E. Biancolini, C. Del Bene, T. Larsson, et al., "Evaluation of go-kart aerodynamic efficiency using CFD, RBF mesh morphing and lap time simulation," vol. 5, no. 3-4, 2017, doi: 10.1504/IJAD.2016.083375.

[4] F. F. Semeraro and P. Schito, "Numerical Investigation of the Influence of Tire Deformation and Vehicle Ride Height on the Aerodynamics of Passenger Cars," *Fluids*, vol. 7, no. 2, p. 47, Jan. 2022, doi: 10.3390/fluids7020047.

[5] M. Aultman, Z. Wang, R. Auza-Gutierrez, et al., "Evaluation of CFD methodologies for prediction of flows around simplified and complex automotive models," *Comput. Fluids*, vol. 236, p. 105297, Mar. 2022, doi: 10.1016/j.compfluid.2021.105297.

[6] C. Zhang, C. P. Bounds, L. Foster, et al., "Turbulence Modeling Effects on the CFD Predictions of Flow over a Detailed Full-Scale Sedan Vehicle," *Fluids*, vol. 4, no. 3, p. 148, Aug. 2019, doi: 10.3390/fluids4030148.

[7] F. F. Buscariolo, G. R. S. Assi, and S. J. Sherwin, "Computational study on an Ahmed Body equipped with simplified underbody diffuser," *J. Wind Eng. Ind. Aerodyn.*, vol. 209, p. 104411, Feb. 2021, doi: 10.1016/j.jweia.2020.104411.

[8] H. Zhou, W. Zhang, T. Huang, et al., "Numerical Analysis of the Aerodynamic Performance of an Ahmed Body Fitted with Spoilers of Different Opening Areas," *Fluid Dyn. Mater. Process.*, vol. 21, no. 5, pp. 1113-1131, 2025, doi: 10.32604/fdmp.2025.064991.

[9] A. Marrel and B. Iooss, "Probabilistic surrogate modeling by Gaussian process: A review on recent insights in estimation and validation," *Reliab. Eng. Syst. Saf.*, vol. 247, p. 110094, Jul. 2024, doi: 10.1016/j.ress.2024.110094.

[10] J. P. C. Kleijnen, "Regression and Kriging metamodels with their experimental designs in simulation: A review," *Eur. J. Oper. Res.*, vol. 256, no. 1, pp. 1-16, Jan. 2017, doi: 10.1016/j.ejor.2016.06.041.

[11] D. Zhan and H. Xing, "Expected improvement for expensive optimization: a review," *J. Glob. Optim.*, vol. 78, no. 3, pp. 507-544, Nov. 2020, doi: 10.1007/s10898-020-00923-x.

[12] X. Hu, P. Ma, S. Li, et al., "The Optimization of Space-Filling and Orthogonality for Latin Hypercube Design Using a Local Search-Based NSGA-II," *J. Stat. Theory Pract.*, vol. 19, no. 1, p. 12, Mar. 2025, doi: 10.1007/s42519-025-00430-w.

[13] L. Wang, Q. Xiao, and H. Xu, "Optimal maximin L1-distance Latin hypercube designs based on good lattice point designs," *Ann. Stat.*, vol. 46, no. 6B, Dec. 2018, doi: 10.1214/17-AOS1674.

[14] J. Yang, H. Chen, D. K. J. Lin, et al., "Construction of sliced maximin-orthogonal Latin hypercube designs," *Stat. Sin.*, 2016, doi: 10.5705/ss.2013.352.

[15] B. Shahriari, K. Swersky, Z. Wang, et al., "Taking the Human Out of the Loop: A Review of Bayesian Optimization," *Proc. IEEE*, vol. 104, no. 1, pp. 148-175, Jan. 2016, doi: 10.1109/JPROC.2015.2494218.

[16] F. Berkenkamp, A. Krause, and A. P. Schoellig, "Bayesian optimization with safety constraints: safe and automatic parameter tuning in robotics," *Mach. Learn.*, vol. 112, no. 10, pp. 3713-3747, Oct. 2023, doi: 10.1007/s10994-021-06019-1.

[17] "The k-ω Shear-Stress Transport (SST) Turbulence Model," in *A New Hypothesis on the Anisotropic Reynolds Stress Tensor for Turbulent Flows*, vol. 120, in Fluid

Mechanics and Its Applications, vol. 120. , Cham: Springer International Publishing, 2019, pp. 57-66. doi: 10.1007/978-3-030-13543-0_3.

[18] H. Ma, Y. Zhang, S. Sun, et al., "A comprehensive survey on NSGA-II for multi-objective optimization and applications," *Artif. Intell. Rev.*, vol. 56, no. 12, pp. 15217-15270, Dec. 2023, doi: 10.1007/s10462-023-10526-z.

[19] O. Cuate and O. Schütze, "Pareto Explorer for Finding the Knee for Many Objective Optimization Problems," *Mathematics*, vol. 8, no. 10, p. 1651, Sep. 2020, doi: 10.3390/math8101651.

[20] E. Ruban.L, I. V. Kennet Thomas, L. M. Dicson .V, D. B.S, et al., "A Study on the effect of fairing designs of Go Kart on its performance using CFD analysis," *Int. Res. J. Adv.*, vol. 2, no. 9, pp. 21-29, Sep. 2020, doi: 10.47392/irjash.2020.142.